J. Fluid Mech. (1998), *vol.* 376, *pp.* 37–51. Printed in the United Kingdom

Role played by the interfacial shear in the instability mechanism of a viscous liquid jet surrounded by a viscous gas in a pipe

By S. P. LIN AND J. N. CHEN

Department of Mechanical and Aeronautical Engineering, Clarkson University, Potsdam, NY 13699-5725, USA

(Received 13 April 1998 and in revised form 23 June 1998)

The role of interfacial shear in the onset of instability of a cylindrical viscous liquid jet in a viscous gas surrounded by a coaxial circular pipe is elucidated by use of an energy budget associated with the disturbance. It is shown that the shear force at the liquid–gas interface retards the Rayleigh-mode instability which leads to the breakup of the liquid jet into drops of diameter comparable to the jet diameter, due to capillary force. On the other hand the interfacial shear and pressure work in concert to cause the Taylor-mode instability which leads the jet to break up into droplets of diameter much smaller than the jet diameter. While the interfacial pressure plays a slightly more important role than the interfacial shear in amplifying the longer-wave spectrum in the Taylor mode, the shear stress plays the main role of generating the disturbances of shorter wavelength.

1. Introduction

A good knowledge of jet instability is relevant to many industrial processes including spray formation in internal combustion engines, ink jet printing, jet cutting and spray coating. References on specific industrial applications can be found in many articles cited in a recent review article by Lin & Reitz (1998). The interfacial shear also plays an important role in environmental fluid mechanics, such as wind-generated waves (Benjamin 1959; Miles 1993).

Plateau (1873) observed that a cylindrical liquid jet tends to break up into equal segments of length which is nine times the jet radius. The spherical drops formed from these segments give the minimum surface energy for the same jet volume. Neglecting the effects of gravity and ambient gas, Rayleigh (1879) showed that the origin of the jet breakup is the hydrodynamic instability. He introduced into the jet infinitesimal disturbances that may grow or decay everywhere in the jet at the same rate. He found that the fastest growing disturbances had a wavelength equalling nine times the jet radius. Weber (1931) and Chandrasekhar (1961) found that the liquid viscosity has only stabilizing effects of reducing the breakup rate and increasing the drop size. Chandrasekhar (1961) also proved that the mechanism of Rayleigh jet instability is capillary pinching. Keller, Rubinow & Tu (1972) observed that these theories were based on the assumption that the disturbances are temporally growing, while the observed disturbances actually grow in space in the flow direction. They extended Rayleigh's analysis to spatially growing disturbances and found that Rayleigh's results are relevant only to the case of large values of the Weber number which is the ratio of the liquid inertia force to the surface tension force per unit area of the interface. For

a Weber number of order one or smaller they found a new mode of faster growing disturbances of much larger wavelength than those of the Rayleigh mode. They conjectured that this new mode of disturbances had not been observed because of its extremely long wavelength. Leib & Goldstein (1986*a*, *b*) showed that this new mode is actually associated with the absolute instability, and the Rayleigh mode is associated with the convective instability. The disturbances can only be convected downstream in a convectively unstable jet, but in an absolutely unstable jet the disturbances are propagated in the downstream as well as in the upstream directions. Attempts have been made to capture an image of absolutely unstable jets (Monkewitz 1990). Only recently have clear images of absolutely unstable jet been reported, by Vihinen, Honohan & Lin (1997). The transition from drop formation to dripping of a liquid jet was conjectured earlier to be related to the transition from a convective to an absolute instability by Lin & Lian (1989), and by Monkewitz (1990). This conjecture was discussed recently by LeDizes (1997) in the light of global absolute instability.

In the above mentioned theories, the predicted drop sizes are of the same order as the jet diameter. Thus, these theories cannot be applied to the atomization phenomenon which is the breakup of a liquid jet into droplets much smaller than the jet diameter. To explain the atomization process, Taylor (1963) took the gas density into account. He considered the limiting case of an infinitely thick jet and extremely small gas-to-liquid density ratio. Taylor's analysis for the case of temporally growing disturbances was extended by Lin & Kang (1987) to the case of spatially growing disturbances in a dense gas.

Unified theories which delineate both the Rayleigh and the Taylor modes of instability with the same characteristic equation have been advanced by Sterling & Sleicher (1975) for the case of temporally growing disturbances, and by Lin & Lian (1989, 1990) for the case of spatio–temporal disturbances. The effect of gas viscosity was taken into account only approximately in these theories. The gas viscosity was fully included in the stability analysis of Lin & Ibrahim (1990), and Lin & Lian (1993). They solved the problem with an eigenfunction expansion. However, they did not elucidate the precise roles of interfacial shear force relative to all other forces in the jet breakup. To fill in this information gap, we calculate the power inputs due to all forces which participate in causing the kinetic energy of the disturbance to grow in a volume of the liquid jet. The relative importance of each force is identified by comparing it with all other forces in the energy budget, which is formulated in §2. Although the solution of Lin & Lian (1993) provides meaningful eigenvalues, the corresponding eigenvectors are not sufficiently accurate for the evaluation of all items in the energy budget. A more accurate solution is obtained by use of the Chebyshev-collocation method which is described in §3. The sign and numerical values of eleven items in the energy budget are determined for a wide range of relevant flow parameters. The results are presented in §4 where the roles of surface tension force, the pressure fluctuation and the normal and tangential viscous forces in the jet instability is discussed. In particular the role of the interfacial shear in the Rayleigh and Taylor modes of jet instability is elucidated.

2. Formulation

Consider the instability of an incompressible Newtonian liquid jet of radius R_1. The jet is surrounded by a viscous gas enclosed in a vertical pipe of radius R_2 which is concentric with the jet. For the jet to maintain a constant radius, the pressure gradients in the steady liquid and gas flows must maintain the same constant value. This will allow the pressure force difference across the liquid–gas interface to be exactly balanced

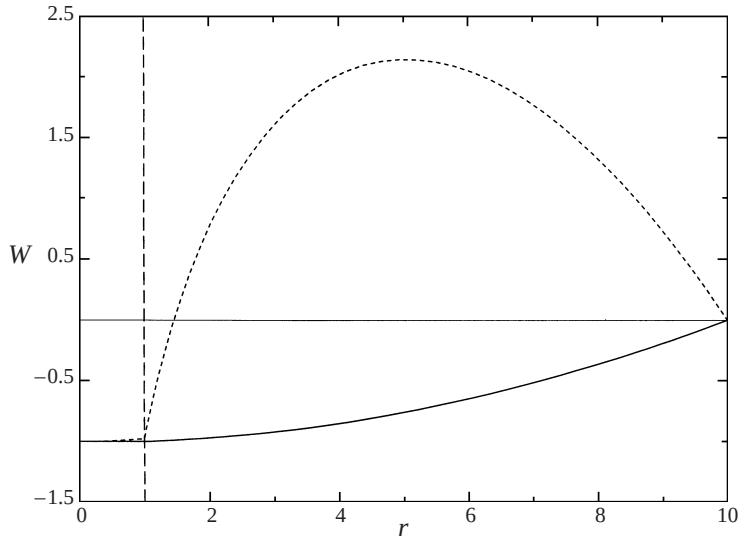

FIGURE 1. Basic flow velocity distribution, $N = 0.018$, $l = 10$, $Re = 1000$. ——, $1/Fr = 0$, $We = 400$, $Q = 0.0013$; -----, $1/Fr = 0.0001$, $We = 4761.9$, $Q = 0.013$; – – –, liquid–gas interface.

by the surface tension force as required. Such coaxial flows, which satisfy exactly the Navier–Stokes equations are given by (Lin & Ibrahim 1990)

$$W_1(r) = -1 + \frac{Nr^2}{[N-(1-l^2)]}\left\{1 - \frac{(1-Q)}{4N} R[2\ln l + (1-l^2)]\right\}, \tag{1a}$$

$$W_2(r) = -\frac{(l^2-r^2)}{[N-(1-l^2)]}\left\{1 - \frac{(1-Q)}{4N} R[2\ln l + (1-l^2)]\right\} + \frac{(1-Q)}{4N} R\left[l^2 - r^2 - 2\ln\left(\frac{l}{r}\right)\right], \tag{1b}$$

in which

$$N = \frac{\mu_2}{\mu_1}, \quad l = \frac{R_2}{R_1}, \quad Q = \frac{\rho_2}{\rho_1}$$

Re is Reynolds number $= \rho_1 W_0 R_1/\mu_1$, and Fr is the Froude number, W_0^2/gR_1, $R = Re/Fr$. The subscript 1 or 2 stands for the liquid or the gas phase respectively, W_0 is the magnitude of the jet velocity on the z-axis, r is the radial distance normalized with R_1, $W(r)$ is the axial velocity distribution normalized with W_0, μ is the dynamic viscosity, ρ is the density, and g is the gravitational acceleration in the negative z-direction. Two different basic flow velocity distributions are given in figure 1. They are obtained in two different regions of the parameter space. The growth rates of the disturbances in these two basic flows are given in figures 2 and 3. The physical mechanisms of jet instability are qualitatively different in these two regions as will be shown in the next section. The existence of these two separate regions can be demonstrated by use of a dimensional argument. There are two obvious characteristic lengths in the problem: the jet radius R_1 and the capillary length $S/\rho_2 W_0^2$, S being the surface tension. If the consequence of instability is the formation of drops whose radii a are comparable with the jet diameter as in the Rayleigh regime, then

$$\frac{a}{R_1} \sim \frac{S}{\rho_1 W_0^2 R_1 Q} = \frac{1}{We\, Q},$$

where We is the Weber number. Thus in the Rayleigh regime $Q \sim We^{-1}$. On the other

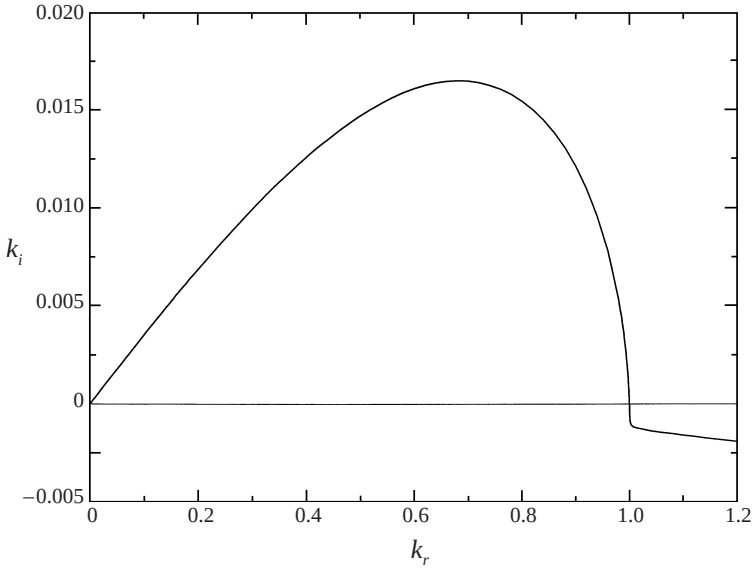

FIGURE 2. Amplification curve for the Rayleigh mode, $Re = 1000$, $1/Fr = 0$, $We = 400$, $Q = 0.0013$, $N = 0.018$, $l = 10$.

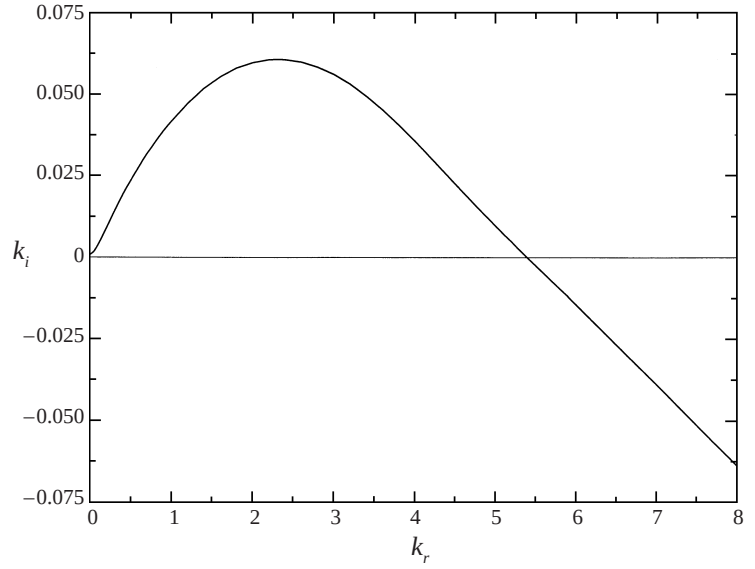

FIGURE 3. Amplification curve for the Taylor mode. $Re = 1000$, $1/Fr = 0.0001$, $We = 4761.9$, $Q = 0.013$, $N = 0.019$, $l = 10$.

hand the Taylor spray droplets scale with $a \quad R_1$, and thus $Q \quad We^{-1}$ according to the above relation. Of course the exact regions of these regimes also depend on other flow parameters.

The onset of instability of the basic flow described by (1) with respect to infinitesimal disturbances is governed by the linearized Navier–Stokes equations

$$\bar{Q}_\alpha \partial_t \boldsymbol{v}_\alpha + \boldsymbol{W}_\alpha \cdot \boldsymbol{\nabla} \boldsymbol{v}_\alpha + \boldsymbol{v}_\alpha \cdot \boldsymbol{\nabla} \boldsymbol{W}_\alpha = -\boldsymbol{\nabla} p_\alpha + Re^{-1} \bar{N}_\alpha \boldsymbol{\nabla} \cdot \boldsymbol{\tau}_\alpha, \tag{2}$$

$$\boldsymbol{\nabla} \cdot \boldsymbol{v}_\alpha = 0 \quad (\alpha = 1, 2), \tag{3}$$

$$\bar{Q}_\alpha = \rho_\alpha / \rho_1, \quad \bar{N}_\alpha = \mu_\alpha / \mu_1,$$

where $\boldsymbol{W}_\alpha$ is the basic flow velocity vector the magnitude of which is given by (1), $\boldsymbol{v}_\alpha$, p_α and t are dimensionless velocity perturbation, pressure disturbance, and time normalized respectively with W_0, $\rho_1 W_0^2$, and R_1/W_0. For the Newtonian fluids considered, the rate of strain $\boldsymbol{\tau}_\alpha$ in (2) is given by

$$\boldsymbol{\tau}_\alpha = [\boldsymbol{\nabla v}_\alpha + (\boldsymbol{\nabla v}_\alpha)^T],$$

where the superscript T stands for transposition.

The boundary conditions at the perturbed liquid–gas interface which is at the radial location $r = 1 + d$ when measured in the unit of R_1, can be linearized by use of the Taylor series expansions of all variables involved about $r = 1$, and retaining only terms of first order in the perturbations. Hence the interfacial conditions are to be evaluated at $r = 1$ with d as an additional unknown. Since the interface is a material surface, d must satisfy at $r = 1$ the kinematic condition

$$d_{,t} + W_1 d_{,z} = u_1, \tag{4}$$

where u is the radial velocity component in the cylindrical coordinates (r, θ, z), and the commas followed by the subscripts denote partial differentiation with respect to the independent variables designated by the subscripts. Other interfacial kinematic conditions are the continuity of the radial and axial components of the velocity across the interface respectively given by

$$[u_\alpha]_2^1 \equiv u_1 - u_2 = 0, \tag{5}$$

$$[W_{\alpha,r}\, d + w_\alpha]_2^1 = 0, \tag{6}$$

where w is the axial component of the perturbation velocity (u, v, w) in the cylindrical coordinate system. Note that the disturbance is considered to be axisymmetric, and thus $v = 0$. The balancing of forces per unit area of interface in tangential and normal directions leads respectively to the dynamic conditions at $r = 1$,

$$[\bar{N}_\alpha \{dW_{\alpha,rr} + w_{\alpha,r} + u_{\alpha,z}\}]_2^1 = 0, \tag{7}$$

$$[p_\alpha - (2/Re)\, \bar{N}_\alpha u_{\alpha,r}]_2^1 + (d + d_{,zz})/We = 0. \tag{8}$$

The boundary condition at the pipe wall is the no-slip condition at $r = R_2/R_1 = l$.

In order to trace the energy sources of the instability, we balance the energy budget in a disturbed liquid jet. A history of the use of energy budgets can be found in Joseph & Renardy (1992). Consider a control volume of the liquid over one wavelength, λ, of the disturbance. Forming the dot product of (2) for liquid ($\alpha = 1$) with $\boldsymbol{v}_1$, integrating over the control volume, using (3) and the Gauss theorem to reduce some of the volume integrals to surface integrals, averaging over one wavelength λ and one wave period $T = 2\pi/\omega_i$, ω_i being the wave frequency, we arrive at the energy equation

$$\frac{1}{T\lambda}\int_0^T \int_V (\partial_t + \boldsymbol{W}_1 \cdot \boldsymbol{\nabla})\, e \,\mathrm{d}V \,\mathrm{d}t = \frac{1}{T\lambda}\int_0^T \int_V \rho_1 \boldsymbol{v}_1 \cdot [\boldsymbol{v}_1 \cdot \boldsymbol{\nabla}\, \boldsymbol{W}_1] \,\mathrm{d}V \,\mathrm{d}t - \frac{1}{T\lambda}\int_0^T \int_A p_1 \boldsymbol{v}_1 \cdot \boldsymbol{n} \,\mathrm{d}A \,\mathrm{d}t$$

$$+ \frac{1}{T\lambda Re}\int_0^T \int_V (\boldsymbol{v}_1 \cdot \boldsymbol{\tau}_1) \cdot \boldsymbol{n} \,\mathrm{d}A \,\mathrm{d}t - \frac{1}{2\,Re\,\lambda T}\int_0^T \int_V \boldsymbol{\tau}_1 \cdot \boldsymbol{\tau}_1 \,\mathrm{d}V \,\mathrm{d}t, \tag{9}$$

where $e = \boldsymbol{v}_1 \cdot \boldsymbol{v}_1/2$ is the disturbance kinetic energy, and V and A stand respectively for the control volume and surface area. Thus the left-hand side of (9) represents the time rate of change of the disturbance kinetic energy in the control volume. The first term on the right-hand side of (9) gives the time rate of mechanical energy transfer between

the disturbance and the basic flow through the Reynolds stress, and the last term gives the mechanical energy dissipation through liquid viscosity. The second and third integrals on the right-hand side of (9) gives respectively the rates of work done by the pressure and the viscous stress of the liquid. These two integrals will be transformed by use of the boundary conditions (7) and (8) to better explain the physics involved. Applying (7) in the evaluation of the surface integrals involving p_1, and applying (8) in the evaluation of the surface integral involving the shear stress, one can write the energy budget (9) as

$$\mathrm{KE} = \mathrm{PRG} + \mathrm{SUT} + \mathrm{SHG} + \mathrm{SHB} + \mathrm{NVG} + \mathrm{SHL} + \mathrm{NVL} + \mathrm{PRL} + \mathrm{REY} + \mathrm{DIS}, \quad (10)$$

where

$$\mathrm{KE} = (2\pi^2/\omega_i\lambda)\int_0^T\int_0^1\int_{-\lambda}^0 (\partial_t + W_1\partial_z)(u_1^2+w_1^2)\,\pi r\,\mathrm{d}z\,\mathrm{d}r\,\mathrm{d}t, \quad (11a)$$

$$\mathrm{PRG} = -(4\pi^2/\omega_i\lambda)\int_{-\lambda}^0 (u_1 p_2)_{r=1}\,\mathrm{d}z, \quad (11b)$$

$$\mathrm{SUT} = (4\pi^2/\lambda\omega_i We)\int_0^T\int_{-\lambda}^0 [u_1(d+d_{,zz})]_{r=1}\,\mathrm{d}z\,\mathrm{d}t, \quad (11c)$$

$$\mathrm{SHG} = (4\pi^2/\lambda\omega_i Re)\int_0^T\int_{-\lambda}^0 Nw_1(w_{2,r}+u_{2,z})_{r=1}\,\mathrm{d}z\,\mathrm{d}t, \quad (11d)$$

$$\mathrm{SHB} = (4\pi^2/\lambda\omega_i Re)\int_0^T\int_{-\lambda}^0 w_1\,\mathrm{d}(NW_{2,rr}-W_{1,rr})_{r=1}\,\mathrm{d}z\,\mathrm{d}t, \quad (11e)$$

$$\mathrm{NVG} = (4\pi^2 N/\lambda\omega_i Re)\int_0^T\int_{-\lambda}^0 [2u_1 u_{2,r}]_{r=1}\,\mathrm{d}z\,\mathrm{d}t, \quad (11f)$$

$$\mathrm{SHL} = (4\pi^2/\lambda\omega_i Re)\int_0^T\int_0^1 [u_1(w_{1,r}+u_{1,z})]_{z=-\lambda}^{z=0} r\,\mathrm{d}r\,\mathrm{d}t, \quad (11g)$$

$$\mathrm{NVL} = (4\pi^2/\lambda\omega_i Re)\int_0^T\int_0^1 2[w_1 w_{1,z}]_{z=-\lambda}^{z=0}\,\mathrm{d}r\,\mathrm{d}t, \quad (11h)$$

$$\mathrm{PRL} = -(4\pi^2/\lambda\omega_i)\int_0^T\int_0^1 [w_1 p_1]_{z=-\lambda}^{z=0} r\,\mathrm{d}r\,\mathrm{d}t, \quad (11i)$$

$$\mathrm{REY} = -(4\pi^2/\lambda\omega_i)\int_0^T\int_0^1\int_{-\lambda}^0 u_1 w_1 W_{1,r}\, r\,\mathrm{d}z\,\mathrm{d}r\,\mathrm{d}t, \quad (11j)$$

$$\mathrm{DIS} = -(4\pi^2/\lambda\omega_i Re)\int_0^T\int_0^1\int_{-\lambda}^0 [2(u_{1,r})^2 + 2(w_{1,z})^2 + (w_{1,r}+u_{1,z})^2]\, r\,\mathrm{d}z\,\mathrm{d}r\,\mathrm{d}t. \quad (11k)$$

Each term in (10) represents the phase-averaged time rate of change of a physically distinctive factor per unit length of the liquid control volume enclosed by the interface of length λ on the side and by the two circular lids at $z = 0$ and $-\lambda$. In (10) KE is the time rate of change of the disturbance kinetic energy. The last term DIS is the rate of mechanical energy dissipation through viscosity in the volume, which tends to reduce KE as it is always negative. The energy transfer between the disturbance and the basic flow through the Reynolds stress is represented by REY, the sign of which depends on the flow parameters. The rest of the surface integrals in (10) represent various rates of

work done on the control surface. PRG represents the rate of work done by the gas pressure fluctuation on the liquid jet, if it is positive. If it is negative, the work is done by the liquid jet on the surrounding gas at the expense of the disturbance kinetic energy. The same sign convention is followed by the rest of the work terms. SUT is the rate of work done by the surface tension. SHG is the rate of work done by the shear stress exerted by the fluctuating gas at the interface. SHB is the rate of work done by the shear stress associated with the basic flow distortion caused by the interfacial displacement. NVG represents the rate of work done by the normal viscous stress exerted by the fluctuating gas at the interface. SHL and NVL represent respectively the rates of work done by the tangential and normal components of the viscous stress at the top and bottom ends of the control volume. The rate of the pressure work at the top and bottom ends of the control volume is given by PRL.

Each integral on the right-hand side of (10) represents a different physical factor which affects the instability of the liquid jet. Therefore the relative magnitude as well as the sign of each term must be evaluated. To achieve this, we must carry out the stability analysis which provides the functions appearing in the integrands of (10). An accurate eigenvector solution is obtained by use of the Chebyshev-collocation method (Boyd 1989) which is described in the next section. The eigenfunctions obtainable from the results of Lin & Ibrahim (1990) and Lin & Lian (1993) are not sufficiently accurate for the present purpose.

3. Stability analysis

The onset of instability of the basic flow with respect to axisymmetric disturbances is considered. Equation (3) allows one to express the radial and axial components of the velocity disturbance in terms of the Stokes stream function ψ_α as

$$u_\alpha = \frac{1}{r}\psi_{\alpha,z}, \quad w_\alpha = -\frac{1}{r}\psi_{\alpha,r}. \tag{12}$$

Arbitrary Fourier components of ψ_α and the corresponding pressure and interfacial displacement d can be written as

$$[\psi_\alpha(r,z,t), p_\alpha(r,z,t), d(z,t)] = [\phi_\alpha(r), \zeta_\alpha(r), \xi]\, \mathrm{e}^{\mathrm{i}kz+\omega t}, \tag{13}$$

where $[\phi_\alpha, \zeta_\alpha, \xi]$ is the perturbation amplitude corresponding to the complex wavenumber $k = k_r + \mathrm{i}k_i$ and the complex wave frequency $\omega = \omega_r + \mathrm{i}\omega_i$. Substitution of the Fourier mode solution into the curle of the linearized Navier–Stokes equation results in the Orr–Sommerfeld equation (Drazin & Reid 1981)

$$\left(\omega - \frac{\nu_\alpha}{\nu_1}\frac{1}{Re}\mathrm{E}^2\right)\mathrm{E}^2\phi_\alpha(r) + \mathrm{i}kW_\alpha(r)\,\mathrm{E}^2\phi_\alpha(r) - \mathrm{i}kr\frac{\mathrm{d}}{\mathrm{d}r}\left[\frac{1}{r}\frac{\mathrm{d}W_\alpha}{\mathrm{d}r}\right]\phi_\alpha(r) = 0, \tag{14}$$

where

$$\mathrm{E}^2 \equiv \frac{\mathrm{d}^2}{\mathrm{d}r^2} - \frac{1}{r}\frac{\mathrm{d}}{\mathrm{d}r} - k^2. \tag{15}$$

The boundary condition at the vertical pipe wall $r = l$ is the no-slip condition,

$$\phi_2(l) = 0, \tag{16}$$

$$\mathrm{D}\phi_2(l) = 0, \quad \mathrm{D} \equiv \frac{\mathrm{d}}{\mathrm{d}r}. \tag{17}$$

By use of (12) and (13), the boundary conditions at the interface (4), (5), (6), (7) and (8) can be written respectively as

$$ik\phi_1 = [\omega + ikW_1(1)]\,\xi, \tag{18}$$

$$[\phi_\alpha]_2^1 \equiv \phi_1(1) - \phi_2(1) = 0, \tag{19}$$

$$[D\phi_\alpha - \xi DW_\alpha]_2^1 = 0, \tag{20}$$

$$\left[\frac{\mu_\alpha}{\mu_1}(E^2 + 2k^2)\,\phi_\alpha - \frac{\rho_\alpha}{\rho_1} R\xi\right]_2^1 = 0, \tag{21}$$

$$\left[\zeta_\alpha - \frac{2ik}{Re}\frac{\mu_\alpha}{\mu_1}(D\phi_\alpha - \phi_\alpha)\right]_2^1 + \xi(1-k^2)/We = 0, \tag{22}$$

where the pressure amplitude can be obtained from the linearized Navier–Stokes equation and is given by

$$ik[\zeta_\alpha]_2^1 = \left[\frac{\rho_\alpha}{\rho_1}(\omega + ikW_a)\,D\phi_\alpha - ik\left(\frac{\rho_\alpha}{\rho_1}\right)\phi_\alpha DW_a - \frac{1}{Re}\left(\frac{\mu_\alpha}{\mu_1}\right)DE^2\phi_\alpha\right]_2^1. \tag{23}$$

The disturbance along the axis $r = 0$ must be bounded. It follows from (12) that

$$\phi_1(0) = 0, \tag{24}$$

$$D\phi_1(0) = 0. \tag{25}$$

Equations (14)–(25) constitute an eigenvalue problem.

The solution for ϕ_α will be obtained by use of the collocation method applying the Chebyshev polynomials as the cardinal function of Lagrange. First we map the liquid region $r \in [0, 1]$ into the Chebyshev space $y \in [-1, 1]$ by use of the linear transformation

$$r = \tfrac{1}{2}(y+1), \tag{26}$$

and map the gas region $r \in [1, l]$ into $y \in [1, -1]$ by the transformation

$$r = 1 - \frac{(l-1)}{2}(y-1). \tag{27}$$

It follows from (26) and (27) that the transformed Orr–Sommerfeld equation in y remains the same except that the pth derivative in r in (14) must be replaced by

$$\frac{d^p}{dr^p} = q_\alpha^p \frac{d^p}{dy^p},$$

where

$$q_1 = 2 \quad \text{for the liquid domain,}$$

$$q_2 = \frac{2}{1-l} \quad \text{for the gas domain.}$$

The same modification must be made in the boundary conditions. The pipe axis and the pipe wall are now both at $y = -1$, and the interface is at $y = 1$. The solution for $\phi_\alpha(y)$ will be expanded as

$$\phi_\alpha(y) = \sum_{j=0}^{N_\alpha} h_{\alpha j}(y)\,\phi_\alpha(y_{\alpha,j}), \tag{28}$$

$$h_{\alpha j}(y) = \frac{(-1)^{j+1}(1-y^2)}{C_j N_\alpha^2 (y - y_{\alpha,j})} T'_{N_\alpha}(y),$$

$$C_0 = C_{N_\alpha} = 2, \quad C_j = 1 \quad \text{for} \quad 0 < j < N_\alpha,$$

where $h_{\alpha j}$ is the Lagrange cardinal function, T_{N_α} is the Chebyshev polynomial and the prime denotes differentiation with respect to y, and the $y_{\alpha,j}$ are the Gauss–Lobatto collocation points (Boyd 1989) given by

$$y_{\alpha j} = \cos\left(\frac{\pi j}{N_\alpha}\right), \quad j = 0, 1, \ldots, N_\alpha. \tag{29}$$

The method of evaluation of the derivatives of ϕ at the collocation points can be found in Boyd (1989). Substitution of ϕ in (28) and its derivatives into the transformed Orr–Sommerfeld equation results in an equation of (N_1+N_2+2) unknown $\phi_{\alpha,j}$. An additional unknown ξ appears in the boundary conditions. Hence there are (N_1+N_2+3) unknowns. The resulting system evaluated at $y_{\alpha,i}$ $(i = 2, 3, \ldots, N_\alpha-2)$ provides $(N_\alpha-3)$ equations from the Orr–Sommerfeld equation for each α, and nine equations from the boundary conditions. The number of equations has been made the same as the number of unknowns by not evaluating the Orr–Sommerfeld equation at $y_{\alpha,i}(i = 0, 1, N_\alpha-1, N_\alpha)$. This is the so-called Lanczos method (1956). The vanishing of the determinant of the coefficient matrix of the eigenvector $\phi_{\alpha,j}$ gives the characteristic equation. The characteristic equation has the form

$$(A_{ij}-\omega B_{ij})\,\phi_j = 0, \tag{30}$$

where A_{ij} and B_{ij} are the parts of coefficient matrix arising respectively from the time-independent and time-dependent part of the Orr–Sommerfeld equation and its boundary conditions. For a given set of flow parameters (Re, Fr, We, N, Q, l) the complex eigenvalues (k, ω) are obtained from the characteristic equation. Assuming the jet to be convectively unstable, we assign a value of (k_r, k_i) such that $k_r > 0, k_i < 0$, and obtain ω_r and ω_i with the subroutine DG2LCG in the IMSL library. If $\omega_r > 0$, we keep the same value of k_r but increase the value of k_i and substitute the new value of (k_r, k_i) into the characteristic equation, and then solve for (ω_r, ω_i) again with the same subroutine. We repeat the same computation until a point $(\omega_r = 0, k_i > 0)$ is reached from the domain $\omega_r > 0, k_i < 0$. We repeat the same procedure for increasing values of k_r, and obtain the spatial amplification curve $(\omega_r = 0, k_i > 0)$ over a range of k_r. This procedure allows us to ascertain that the amplification curve in the complex k-plane can be reached from the domain $k_i < 0, \omega_r > 0$ so that the causality condition, i.e. the condition that the disturbance does not exist in $t < 0$, can be satisfied (Bers 1983). This procedure breaks down in a certain parameter space when saddle point and branch point singularities appear in the complex k- and ω-planes. The jet is then absolutely unstable (Bers 1983; Briggs 1964).

Some numerical results of stability analysis were given in figures 1–3 in §2. To test the possible syntax and computer program errors, the results for the special cases included in the present problem are checked against the known results of axisymmetric Poiseuille flow (Davey & Drazin 1969) and core–annular flow (Preziosi, Chen & Joseph 1989). The numbers of terms retained in (28) are systematically increased until desired significant digits are obtained for the eigenvalue, eigenvector, and its derivatives. A typical example of the convergence test is given in table 1 in which six, five and four significant digits are obtained for the eigenvalue, eigenvector, and its fourth derivative. The eigenvectors and their derivatives corresponding to the calculated eigenvalues are obtained by use of the IMSL subroutine G2CCG. The results of the energy budget will be discussed in §4 after the following results on instability are discussed.

Figure 2 gives a spatial amplification curve $\omega_r = 0$ for the flow parameters specified in the figure caption. Q and We are so chosen that $Q \sim We^{-1}$ to yield the Rayleigh

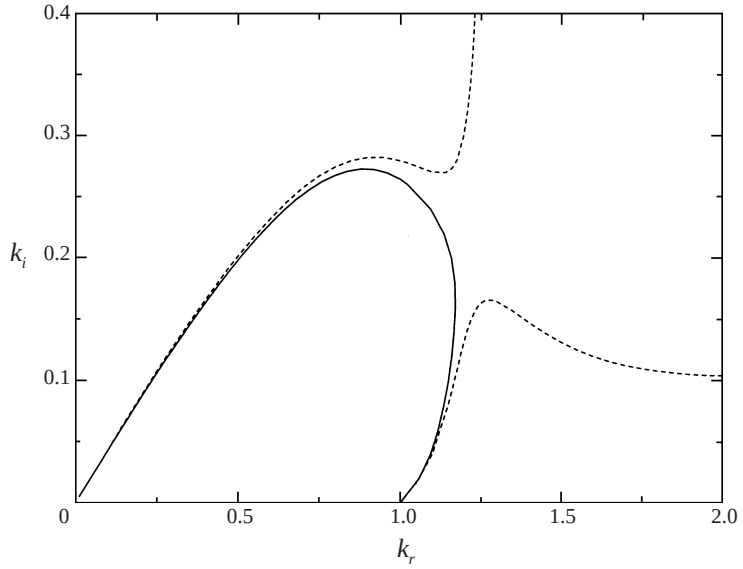

FIGURE 4. Emergence of a saddle point. $Re = 200$, $1/Fr = 0$, $Q = 0.0013$, $N = 0.018$, $l = 10$. ——, $We = 2.703$; -----, $We = 2.632$.

N_1	N_2	k_i	ω_i	$\phi_1(1)$	$\phi_2^{iv}(1)$
25	60	0.08025	4.6843	−0.00370	−55260
20	70	0.08112	4.6834	−0.00389	−56280
30	70	0.08112	4.6834	−0.00389	−56280
20	80	0.08106	4.6833	−0.00391	−56340
20	90	0.08105	4.6833	−0.00391	−56340
30	90	0.08106	4.6833	−0.00391	−56340
20	100	0.08105	4.6833	−0.00301	−56340

TABLE 1. Convergence test: $Re = 500$, $Fr^{-1} = 0.0005$, $We = 10^5$, $Q = 0.0013$, $N = 0.018$, $l = 10$, $k_r = 5.0$.

mode. This curve can be approached from below starting with $\omega_r > 0$, $k_i < 0$ for a given k_i. Hence the liquid jet for the given flow parameters is convectively unstable. The maximum spatial amplification rate k_{im} occurs at the wavenumber $k_{rm} = 0.684$ which is slightly smaller than the wavenumber for the maximum temporal growth rate found by Rayleigh for an inviscid jet in vacuum. The cutoff wavenumber below which the viscous jet is stable is $k_{rc} = 1$. This value is the same as that found by Rayleigh, except the jet is neutrally stable for the inviscid case. Another spatial amplification curve for a different set of flow parameters is given in figure 3. Q and We are so chosen that $Q \quad We^{-1}$ to yield the Taylor mode. The jet is again convectively unstable. However, both k_{rm} and k_{rc} are much larger than those in figure 1. Hence the unstable disturbances with a broader bandwidth of wavelength manifest themselves at the onset of instability which leads to the formation of smaller droplets. Although the jets specified in figures 2 and 3 are both convectively unstable, the physical origins of instability are totally different as will be explained in the next section.

Figure 4 shows the emergence of a saddle point singularity in the (k_r, k_i)-plane. At $We = 2.703$ and the rest of flow parameters specified in the figure caption, the jet is convectively unstable. The spatial amplification curve is given by the solid line. When

the value of We is decreased to 2.632 while the rest of flow parameters remain the same a saddle point at $k_r = 1.2162$, $k_i = 0.21658$ appears, and the jet becomes absolutely unstable. The curve $\omega_r = 0$ has two branches shown as dotted lines; ω_i increases with increasing k_r along the upper branch but decreases along the lower branch. Thus for the disturbances characterized by the upper and lower branches the wave packet propagates respectively upstream and downstream as they grow. The jet is absolutely unstable. The physical mechanism of absolute instability is basically the same as that of the Rayleigh-mode convective instability, as will be shown in the next section.

4. Mechanism of jet breakup

All items in the energy budget (10) have been evaluated by integrating the integrands obtained in the previous section by use of the Gauss quadrature method and the Runge–Kutta method. The two methods are implemented respectively by use of the IMSL subroutines DQDAGS and DIVPRK. The results obtained by the two methods are compared for possible syntax or program error. All integrals in (10) are evaluated independently from one another. The comparison of the sum of integrals on the right-hand side of (10) with the integral on the left-hand side provides an independent check of the overall numerical accuracy. Moreover, the number of terms in the eigenfunction expansions were varied in the integrands of (10) to ascertain the numerical accuracy. A minimum of three-significant-digit accuracy is maintained in the results to be presented.

The energy budget in a liquid jet perturbed by the disturbances whose amplification rates are depicted in figure 2 is displayed in table 2. All items of the energy budget, except SHB which is zero in this case of $Fr^{-1} = 0$, as can be seen from (1) and (10), are listed for various wavenumbers for comparisons. The wavenumbers cover both stable and unstable disturbances. All items are normalized with the maximum kinetic energy term occurring at $k_{rm} = 0.684$. It is seen from this table that the positive rates of change of the disturbance kinetic energy are mainly due to the work done by the surface tension on the control liquid volume. Although the viscous normal stress exerted by gas represented by NVG as well as the normal stress work represented by PRL and NVL at the top and bottom of the cylindrical liquid column also contribute to the growth of the unstable disturbance, they are several orders of magnitude smaller than the surface tension term SUT. The major factor which resists disturbance growth is viscous dissipation. The pressure and the shear stress exerted by the gas at the liquid–gas interface are also significant factors against instability. Although the liquid tangential viscous stress represented by SHL and the bulk Reynolds stress represented by REY also contributed to drain the kinetic energy from the disturbance, they are many order of magnitudes smaller than DIS. However the sum of all negative terms is not sufficiently large in magnitude to counter the destabilizing effect of the surface tension. Thus the mechanism of the instability of a viscous liquid jet in a viscous gas by the Rayleigh mode remains capillary pinching which was demonstrated by Chandrasekhar (1961) who considered an inviscid liquid jet in vacuum. An inviscid Rayleigh jet is neutral with respect to disturbances of wavenumber larger than the cutoff wavenumber $k_{rc} = 1$. Thanks to viscous dissipation these disturbances are actually damped according to table 2. The stabilizing and destabilizing factors retain their signs in the range of k_r given in table 2, except for the Reynolds stress term, although some energy is transferred from the mean flow to the disturbances of wavelength shorter than $2\pi R_1$ the growth of which is suppressed by viscous, dissipation. Note that the change of SUT with k_r is not monotonic, and its maximum does not occur at k_{rm}. In fact neither do any

k_r	KE	REY ($\times 10^{-4}$)	SUT	PRL ($\times 10^{-3}$)	PRG ($\times 10^{-3}$)	NVG ($\times 10^{-3}$)	DIS ($\times 10^{-1}$)	SHL ($\times 10^{-5}$)	NVL ($\times 10^{-4}$)	SHG ($\times 10^{-2}$)
0.140	0.127	−0.120	0.129	0.0159	0.0335	0.00939	−0.0128	−0.00791	0.0245	−0.115
0.200	0.248	−0.234	0.254	0.0734	−0.206	0.0252	−0.0362	−0.0225	0.0674	−0.178
0.300	0.503	−0.474	0.520	0.181	−0.323	0.0795	−0.113	−0.0676	0.197	−0.287
0.400	0.771	−0.721	0.804	0.420	−0.506	0.169	−0.241	−0.134	0.380	−0.384
0.500	0.980	−0.910	1.03	0.736	−0.949	0.280	−0.407	−0.210	0.558	−0.452
0.600	1.06	−0.984	1.14	0.650	−1.28	0.389	−0.592	−0.292	0.654	−0.473
0.684	1.00	−0.931	1.09	1.19	−1.43	0.452	−0.680	−0.366	0.622	−0.445
0.700	0.973	−0.908	1.06	2.15	−1.45	0.458	−0.716	−0.380	0.603	−0.434
0.800	0.697	−0.681	0.781	0.882	−1.31	0.433	−0.681	−0.451	0.398	−0.327
0.900	0.296	−0.347	0.353	0.496	−0.718	0.264	−0.457	−0.388	0.131	−0.159
1.100	−0.057	3.00	0.0672	1.47	−2.47	1.47	−1.20	−1.09	0.00318	−0.476
1.200	−0.160	7.71	0.182	5.79	−6.71	3.36	−3.34	−3.70	0.0105	−1.08

TABLE 2. Energy budget for the Rayleigh mode: $Re = 1000$, $Fr^{-1} = 0.0$, $We = 400$, $Q = 0.0013$, $N = 0.018$, $l = 10$.

k_r	KE	REY	SUT	PRL	PRG	NVG	DIS	SHL ($\times 10^{-4}$)	NVL ($\times 10^{-4}$)	SHG	SHB ($\times 10^{-1}$)
0.1	0.00298	5.12×10^{-5}	2.34×10^{-4}	6.95×10^{-5}	0.00184	2.77×10^{-6}	-1.18×10^{-4}	-1.78×10^{-4}	0.000429	4.4×10^{-4}	0.00551
1.0	0.536	−0.0247	3.92×10^{-4}	0.0193	0.484	−0.00194	−0.0833	−3.87	0.829	0.164	−0.178
2.0	0.993	−0.0544	−0.219	0.0282	1.23	−0.0196	−0359	−16.7	1.89	0.441	−0.424
2.3	1.00	−0.0573	−0.358	0.0262	1.42	−0.0309	−0.467	−19.2	1.87	0.531	−0.499
3.0	0.826	−0.0458	−0.762	0.0198	1.76	−0.0756	−0.729	−17.4	1.38	0.744	−0.677
4.0	0.507	0.0154	−1.12	0.0161	2.04	−0.223	−1.14	0.391	0.490	1.02	−0.924
5.0	0.262	0.0292	−0.585	0.0101	2.43	−0.553	−2.18	3.66	0.0544	1.26	−1.18
6.0	−0.809	−0.118	1.43	−0.0312	3.07	−1.14	−5.30	−1.60	0.217	1.51	−1.50
8.0	−10.8	−1.03	14.1	−0.406	4.86	−3.30	−26.5	256.0	12.0	2.00	−2.28

TABLE 3. Energy budget for Taylor mode: $Re = 1000$, $Fr^{-1} = 0.0001$, $We = 4761.9$, $Q = 0.013$, $N = 0.019$, $l = 10$.

k_r	KE	REY	SUT	PRL ($\times 10^{-2}$)	PRG	NVG	DIS	SHL ($\times 10^{-3}$)	NVL ($\times 10^{-4}$)	SHG	SHB
1.00	0.273	−0.534	-6.06×10^{-7}	1.23	0.251	0.00306	−0.115	−0.612	0.892	0.212	−0.0354
2.00	0.676	−0.162	-5.95×10^{-4}	1.94	0.778	−0.00437	−0.548	−3.86	3.10	0.727	−0.117
4.05	1.00	−0.325	-6.82×10^{-3}	0.0668	1.84	−0.157	−2.28	−12.5	4.92	2.24	−0.297
6.00	0.848	−0.378	−0.0202	−1.41	2.64	−0.481	−4.43	−16.2	3.79	4.02	−0.456
10.0	0.402	−0.321	−0.0607	−1.61	3.26	−1.23	−9.03	−12.1	1.22	8.55	−0.738
15.0	0.191	−0.215	−0.113	−0.823	2.98	−1.59	−16.2	−5.79	0.295	16.5	−1.07
20.0	0.108	−0.134	−0.149	−0.361	2.36	−1.51	−26.4	−2.49	0.0841	27.3	−1.41
25.0	0.0566	−0.0759	−0.149	−0.129	1.75	−1.29	−39.9	−0.826	0.0212	41.4	−1.75
30.0	0.0196	−0.0329	−0.0861	−0.0238	1.06	−0.901	−56.9	−0.111	0.00235	58.9	−2.09
35.0	−0.00717	−0.00180	0.049	0.00198	0.915	−0.987	−77.2	−0.0193	0.000308	79.7	−2.44

TABLE 4. Energy budget for Taylor mode: $Re = 500$, $Fr^{-1} = 0.0005$, $We = 10^6$, $Q = 0.0013$, $N = 0.018$, $l = 10$.

of the other terms change monotonically, and their maxima do not occur at the same k_r. This indicates the significance of interplay among all items in determining the maximum growth rate.

Table 3 gives the energy budget in a liquid jet corresponding to figure 3 which displays the amplification of disturbances giving rise to Taylor-mode instability. While the surface tension work terms remain positive for wavenumbers smaller than 1 in both Rayleigh and Taylor modes, they become negative for shorter unstable disturbances in the Taylor mode. Hence surface tension is not responsible for initiating the formation of droplets whose radius is smaller than the jet radius. The dominant positive terms are PRG and SHG. Thus the work done by the fluctuating gas pressure and the tangential shear stress at the interface is mainly responsible for the Taylor-mode instability. Other positive terms PRL, SHL, and NVN are at least one order of magnitude smaller than these two terms. Recall that PRG and SHG are negative in table 2. This is the fundamental difference in the origin of instability for the Rayleigh and the Taylor modes. Another fundamental difference is that while the normal component of the gas viscous stress plays a minor role in destabilizing the Rayleigh jet, it plays a major role together with the viscous dissipation and the reverse energy transfer to the mean flow through the Reynolds stress in stabilizing the disturbance of wavenumbers greater than the cutoff wavenumber $k_{rc} = 5.4$. This is clearly displayed in table 3. Although it has been believed that interfacial shear is important for the generation of Taylor-mode instability (Lin & Reitz 1998), and it has been pointed out (Lin & Creighton 1990) that the interfacial pressure fluctuation may be equally important, the relative importance of these two factors has never been quantitatively demonstrated before. Table 3 presents the case in which the gas pressure fluctuation plays a slightly larger role than the interfacial shear. Table 4 presents another case of Taylor mode instability in which the interfacial shear plays a more significant role than the pressure fluctuation. Note that the magnitude of SHG increases more rapidly than that of PRG as k_r is increased and eventually dominates over the gas pressure term for this case. Thus the unstable disturbances near the cutoff wavenumber $k_{rc} = 33.5$ are mainly generated by the shear stress fluctuation with significant help from the gas inertia force manifested in the gas pressure fluctuation.

The energy budget at the saddle point in figure 4 is: $\mathrm{KE} = 0.3321$, $\mathrm{REY} = -0.2639 \times 10^{-4}$, $\mathrm{SUT} = 0.1957$, $\mathrm{PRL} = 0.1702$, $\mathrm{PRG} = -0.7063 \times 10^{-3}$, $\mathrm{NVG} = 0.1890 \times 10^{-3}$, $\mathrm{DIS} = -0.2914 \times 10^{-1}$, $\mathrm{SHL} = -0.5326 \times 10^{-4}$, $\mathrm{NVL} = 0.1226 \times 10^{-2}$, and $\mathrm{SHG} = -0.1027 \times 10^{-2}$. Note that the rate of pressure work done by the liquid at the upper and lower ends of the control volume PRL is increased significantly over that in table 2. Otherwise all of the work terms retain the same qualitative roles. Hence the mechanism of the jet breakup by absolute instability is essentially the same as that of the Rayleigh mode by capillary pinching except the axial jet pressure fluctuation plays an equally important role.

5. Conclusion

The onset of instability in a viscous liquid jet in the presence of a surrounding viscous gas may manifest itself as convective or absolute instability depending on the flow parameters. There are two different modes of convective instability, the Rayleigh and Taylor modes, these two modes are caused by fundamentally different physical mechanisms. The main cause of the Rayleigh-mode instability is capillary pinching which is resisted by the inertia in the form of pressure fluctuation and the viscous shear stress exerted by the gas at the interface. On the other hand, the gas pressure and shear

fluctuations are the main means of supplying energy to the disturbances in the Taylor-mode instability. The surface tension tends to resist the formation of short waves. The unstable disturbances in an absolutely unstable jet propagate both in the upstream and downstream directions, accompanied by a large liquid pressure fluctuation in the axial direction. This pressure fluctuation is of the same order of magnitude as the surface tension term. Capillary pinching remains a dominant source of absolute instability as well as the Rayleigh mode of convective instability.

This work was supported in part by grant No. NAG3-1891 of NASA and DAAH04-93-G0395 of ARO.

REFERENCES

Benjamin, T. B. 1959 *J. Fluid Mech.* **6**, 169.

Bers, A. 1983 In *Handbook of Plasma Physics* (ed. M. Rosenbluth), vol. 1, p. 452. North Holland.

Boyd, J. P. 1989 *Chebyshev and Fourier Spectral Method.* Springer.

Briggs, R. J. 1964 *Electron Stream Interaction with Plasma.* MIT Press.

Chandrasekhar, S. 1961 *Hydrodynamic and Hydromagnetic Stability*, p. 537. Oxford University Press.

Davey, A. & Drazin, P. G. 1969 *J. Fluid Mech.* **36**, 209.

Drazin, P. G. & Reid, W. H. 1981 *Hydrodynamic Stability*. Cambridge University Press.

Huerre, P. & Monkewitz, P. A. 1990 *Ann. Rev. Fluid Mech.* **22**, 473.

Joseph, D. D. & Renardy, Y. Y. 1992 *Fundamental of Two-Fluid Dynamics.* Springer.

Keller, J. B., rubinow, S. I. & Tu, Y. O. 1972 *Phys. Fluids* **16**, 2052.

Lanczos, C. 1956 *Applied Analysis* Prentice-Hall.

Ledizes, S. 1997 *Eur. J. Mech.* B/*Fluids*, **16**, 761.

Leib, S. J. & Goldstein, M. E. 1986*a* *Phys. Fluids* **29**, 952.

Leib, S. J. & Goldstein, M. E. 1986*b*. *J. Fluid Mech.* **168**, 479.

Lin, S. P. & Creighton, B. 1990 *J. Aerosol. Sci. Technol.* **12**, 630.

Lin, S. P. & Ibrahim, E. A. 1990 *J. Fluid Mech.* **218**, 641.

Lin, S. P. & Kang, D. J. 1987 *Phys. Fluids* **30**, 2000.

Lin, S. P. & Lian, Z. W. 1989 *Phys. Fluids* A **1**, 490.

Lin, S. P. & Lian, Z. W. 1990 *AIAA J.* **28**, 120.

Lin, S. P. & Lian, Z. W. 1993 *Phys. Fluids* A **5**, 771.

Lin, S. P. & Reitz, R. D. 1998 *Ann. Rev. Fluid Mech.* **30**, 85.

Miles, J. 1993 *J. Fluid Mech.* **256**, 427.

Monkewitz, P. A. 1990 *Eur. J. Mech.* B/*Fluids*, **9**, 395.

Plateau, J. 1873 *Statique Experimentale et Theorique des Liquids Soumle aux Seule Forces Moleculaire Vols. 1, 2.* Gauthier Villars.

Preziosi, L., Chen, K. & Joseph, D. D. 1989 *J. Fluid Mech.* **201**, 323.

Rayleigh, Lord 1879 *Lond. Math. Soc.* **10**, 4.

Sterling, A. M. & Sleicher, C. A. 1975 *J. Fluid Mech.* **68**, 477.

Taylor, G. I. 1963 *The Scientific Papers of Geoffery Ingram Taylor*, vol. 3, no. 25. Cambridge University Press.

Vihinen, I., Honohan, A. M. & Lin, S. P. 1997 *Phys. Fluids* **9**, 3117.

Weber, C. Z. 1931 *Math. Mech.* **11**, 36.